A NEW TWO-PHASE PRESSURE DROP MODEL FOR POROUS MEDIA IN BOILING CONDITIONS FOR DRYOUT HEAT FLUX PREDICTION

Jin Ho Park, Hyun Sun Park*, and Mooneon Lee
POSTECH
hejsunny@postech.ac.kr
jinho912@postech.ac.kr; hejsunny@postech.ac.kr; lmucjn@postech.ac.kr

ABSTRACT

When a severe accident occurs in nuclear power plants, a porous debris bed which is composed of irregular shaped particles with a size distribution ranging from a few of micrometers to approximately 10 mm, and has macro inhomogeneity can be formed on the reactor cavity floor in the ex-vessel phase. The assurance of the ex-vessel debris bed coolability is crucial to stabilize and terminate severe accident progression because it causes the molten core concrete interaction, which threatens the integrity of the containment building. Thus, it is important to supply water into the heat generating debris bed continuously, the effectiveness of which is determined by the pressure drop through the porous debris bed. For this reason, it is necessary to investigate the pressure drop mechanisms and the resulting heat transfer performance in a debris bed, characterized by geometric parameters. Thus, the objective of present study is to evaluate the adequacy of a new two-phase pressure drop model for porous media under boiling conditions for dryout heat flux prediction, which is proposed by our previous study. Comparison between the experimental data (pressure drop in boiling condition and dryout heat flux) and the values predicted by the proposed model was conducted using the various results of DEBRIS experiments conducted at IKE in Germany and others. In conclusion, the adequacy of the proposed model from our previous study was verified for predicting the pressure drop of two-phase flow in particle beds under boiling conditions, and dryout heat flux prediction.

KEYWORDS
Pressure gradient, two-phase flow, porous media, boiling condition, dryout heat flux

1. INTRODUCTION

A debris bed can be formed in the lower plenum of reactor pressure vessel and the reactor cavity in nuclear power plants when a severe accident occurs. The molten core material can fall into the lower plenum of the reactor pressure vessel and a debris bed can be formed when the core damage occurs. The molten core material may be further released into a water-filled reactor cavity when a severe accident progresses to the ex-vessel phase. While discharging the molten core material into the reactor cavity, the molten core material interacts with water, and it is fragmented into millimeter-sized particles and precipitated as a debris bed on the reactor cavity floor. A debris bed is composed of non-spherical particles with a size distribution ranging from a few of micrometers to approximately 10 mm, and has macro inhomogeneity [1, 2]. In order to stabilize and terminate severe accident progression, the assurance of the ex-vessel debris bed coolability is crucial. Unless the decay heat in the core debris is not removed sufficiently, the once solidified particulate debris may heat up, re-melt and cause the molten core concrete interaction, which threatens the integrity of

the containment building. The cooling can be accomplished by continuously supplying water to the heat generating debris bed, the effectiveness of which is determined by the pressure drop through the porous debris bed. For this reason, it is necessary to investigate the pressure drop mechanisms and the resulting heat transfer performance in a debris bed, characterized by geometric parameters. Thus, the objective of present study is to evaluate the adequacy of a new two-phase pressure drop model [3] for porous media under boiling conditions for dryout heat flux prediction, which is proposed by our previous study through experimental data (2, 3.5, 5 mm diameter particles) and verified by existing various experimental data with the diameter of 3.18–6.35 mm in the superficial air velocity range of 0–0.8 m/s under isothermal conditions.

2. TWO-PHASE PRESSURE DROP FOR POROUS MEDIA [3]

The pressure drop models of a two-phase flow in porous media are expressed by Eqs. (1) and (2) for liquid and gas:

$$-\frac{dp_l}{dz} = \rho_l g + \frac{\mu_l}{KK_{rl}} V_{sl} + \frac{\rho_l}{\eta\eta_{rl}} V_{sl}\left|V_{sl}\right| - \frac{F_i}{s}, \tag{1}$$

$$-\frac{dp_g}{dz} = \rho_g g + \frac{\mu_g}{KK_{rg}} V_{sg} + \frac{\rho_g}{\eta\eta_{rg}} V_{sg}\left|V_{sg}\right| + \frac{F_i}{\alpha}, \tag{2}$$

where $-dp/dz$ represents pressure gradient in porous media when the superficial velocity of fluid is V_{si} (i: phase; l = liquid, g = gas). ρ_i and μ_i are the dynamic density and the viscosity of fluid, respectively. K_{rl}, K_{rg} and η_{rl}, η_{rg} are the relative permeabilities and passabilities of a liquid and gas, respectively. F_i is the interfacial drag between a liquid and gas and s (=$1-\alpha$) is the liquid saturation. K and η, Eqs. (3) and (4) are the permeability, a measure of the flow conductance and the passability, a quality of being passable of porous media, respectively,

$$K = \frac{\varepsilon^3 d_p^2}{C_1(1-\varepsilon)^2}, \tag{3}$$

$$\eta = \frac{\varepsilon^3 d_p}{C_2(1-\varepsilon)}, \tag{4}$$

where C_1 and C_2 are the empirical Ergun constants, d_p and ε are the particle diameter and the bed porosity, respectively. The bed porosity, Eq. (5) is calculated by the mass of particles m_p in a test section, the density of particles ρ_p, and the volume of the test section V_t.

$$\varepsilon = 1 - \frac{\sum(m_p / \rho_p)}{V_t} \tag{5}$$

In order to reduce the uncertainty in predicting pressure gradient of a two-phase flow through a debris bed, especially composed of small-sized particles with a diameter less than or equal to 5 mm, our previous study proposed [3] a new improved model based on the Schmidt model [5] with the modified Ergun constants ($C_1 = 36k_0\tau^2$ and $C_2 = 3\tau(3/2 + 1/\beta^4 - 5/2\beta^2)/4$) [4], which is different from the existing analytical models using the Ergun constants ($C_1 = 150, C_2 = 1.75$). Where k_0 depends upon the shape of the cross-section of the channel for the viscous energy loss term [6], and the general value of $k_0\tau^2 = 5$, τ is the

tortuosity suggested by Yu and Li [7], Eq. (6) where $\beta = 1/(1-\sqrt{1-\varepsilon})$ is the ratio of pore diameter to throat diameter.

$$\tau = \frac{L_t}{L} = \frac{the\ actual\ length\ of\ flow\ path}{the\ straight\ length} = \frac{1}{2}\left[1+\frac{1}{2}\sqrt{1-\varepsilon}+\sqrt{1-\varepsilon}\,\frac{\sqrt{\left(\frac{1}{\sqrt{1-\varepsilon}}-1\right)^2+\frac{1}{4}}}{1-\sqrt{1-\varepsilon}}\right] \quad (6)$$

The formulas of our proposed model are listed in Table I.

Table I. The formulas of proposed model in our previous study [3].

	Flow regime	K_{rg}	η_{rg}	K_{rl}	η_{rl}	F_i
$0<\alpha<\alpha_1$	Bubbly (B)	$\left(\frac{1-\varepsilon}{1-\varepsilon\alpha}\right)^{4/3}\alpha^4$	$\left(\frac{1-\varepsilon}{1-\varepsilon\alpha}\right)^{2/3}\alpha^4$	s^3	s^5	$C_{v,B}=18(\alpha_0 f+\alpha-\alpha_0)$ $C_{i,B}=0.34s^3(\alpha_0 f^2+\alpha-\alpha_0)$ $F_{i,B}=C_{v,B}\frac{\mu_l}{D_b^2\varepsilon}sV_r+C_{i,B}\frac{(s\rho_l+\alpha\rho_g)}{D_b\varepsilon^2}s^2V_r\lvert V_r\rvert$
$\alpha_1<\alpha<\alpha_2$	Transition from bubbly to slug (BS)					$C_{v,BS}=C_{v,B}(1-W)+C_{v,S}W$ $C_{i,BS}=C_{i,B}(1-W)+C_{i,S}W$ $F_{i,BS}=C_{v,BS}\frac{\mu_l}{D_b^2\varepsilon}sV_r+C_{i,BS}\frac{(s\rho_l+\alpha\rho_g)}{D_b\varepsilon^2}s^2V_r\lvert V_r\rvert$
$\alpha_2<\alpha<\alpha_3$	Slug (S)					$C_{v,S}=5.21\alpha,\ C_{i,S}=0.92s^3\alpha$ $F_{i,S}=C_{v,S}\frac{\mu_l}{D_b^2\varepsilon}sV_r+C_{i,S}\frac{(s\rho_l+\alpha\rho_g)}{D_b\varepsilon^2}s^2V_r\lvert V_r\rvert$
$\alpha_3<\alpha<\alpha_4$	Transition from slug to annular (SA)	$\frac{\left(\frac{1-\varepsilon}{1-\varepsilon\alpha}\right)^{4/3}\alpha^3}{\left(W+\frac{1-W}{\alpha}\right)}$	$\frac{\left(\frac{1-\varepsilon}{1-\varepsilon\alpha}\right)^{2/3}\alpha^3}{\left(W+\frac{1-W}{\alpha}\right)}$			$F_{i,SA}=F_{i,S}(1-W)+F_{i,A}W$
$\alpha>\alpha_4$	Annular (A)	$\left(\frac{1-\varepsilon}{1-\varepsilon\alpha}\right)^{4/3}\alpha^3$	$\left(\frac{1-\varepsilon}{1-\varepsilon\alpha}\right)^{2/3}\alpha^3$			$F_{i,A}=\left(\frac{\mu_g}{KK_{rg}}s\alpha V_r+\frac{\rho_g}{\eta\eta_{rg}}s\alpha^2V_r\lvert V_r\rvert\right)(1-\alpha)^4$ $\times\min\left(1,\left(\frac{d_p}{0.006}\right)^2\right)$

The void fraction at the onset of bubble merger α_1, the void fraction at the onset of slug flow α_2, the void fraction at the beginning of slug merger α_3, and the void fraction at the onset of pure annular flow α_4 in Table II are adopted from the results of Schmidt [5]. Furthermore, the interfacial drag F_i and its coefficients (C_v, C_i) according to the flow regime are listed in Table I. Here, the bubble diameter D_b, the relative velocity V_r and the geometric factor f are defined through Eqs. (7)–(9), respectively, where γ is the ratio of bubble diameter D_b and particle diameter d_p.

$$D_b = \min\left(1.35\sqrt{\frac{\sigma}{g(\rho_l-\rho_g)}},\ (\sqrt{2}-1)d_p\right) \quad (7)$$

$$V_r = \frac{V_{sg}}{\alpha} - \frac{V_{sl}}{s} \tag{8}$$

$$f = \frac{1}{2}(1+\gamma)\ln\left(1+\frac{2}{\gamma}\right) \tag{9}$$

For a smooth transition between flow regimes, the weighting function $W(\xi)$ was adopted as Eq. (10).

$$W(\xi) = \xi^2(3-2\xi) \quad \text{where } \xi = \frac{\alpha-\alpha_i}{\alpha_{i+1}-\alpha_i} \tag{10}$$

Eqs. (1) and (2) can be expressed in a dimensionless form as follows:

$$\left(-\frac{dp}{dz}\right)^* = \frac{\rho_l g}{(\rho_l-\rho_g)g} + \frac{F_{pl}^*}{s} - \frac{F_i^*}{s}, \tag{11}$$

$$\left(-\frac{dp}{dz}\right)^* = \frac{\rho_g g}{(\rho_l-\rho_g)g} + \frac{F_{pg}^*}{\alpha} + \frac{F_i^*}{\alpha}, \tag{12}$$

where

$$\left(-\frac{dp}{dz}\right)^* = \frac{-dp/dz}{(\rho_l-\rho_g)g}, \tag{13}$$

$$F^* = \frac{F}{\varepsilon(\rho_l-\rho_g)g}, \tag{14}$$

$$F_{pl} = \varepsilon s\left(\frac{\mu_l}{KK_{rl}}V_{sl} + \frac{\rho_l}{\eta\eta_{rl}}V_{sl}\left|V_{sl}\right|\right), \tag{15}$$

$$F_{pg} = \varepsilon\alpha\left(\frac{\mu_g}{KK_{rg}}V_{sg} + \frac{\rho_g}{\eta\eta_{rg}}V_{sg}\left|V_{sg}\right|\right). \tag{16}$$

Table II. Void fractions for flow pattern boundaries.

	Tung and Dhir, TD [8]	Schmidt, S [5]
α_0	$\frac{\pi}{3}\frac{(1-\varepsilon)}{\varepsilon}\gamma(1+\gamma)[6\beta_r - 5(1+\gamma)]$	-
α_1	$\min\left[0.3,\ 0.6(1-\gamma)^2\right]$	$\frac{\pi/6}{5}(d_p - 0.008) + \alpha_{1,TD}\ (d_p < 8mm)$ $\alpha_{1,TD}\ (d_p > 8mm)$
α_2	$\pi/6 \approx 0.52$	$\frac{\pi/6}{5}(d_p - 0.008) + \alpha_{2,TD}\ (d_p < 8mm)$ $\alpha_{2,TD}\ (d_p > 8mm)$
α_3	0.6	$\frac{\pi/6}{5}(d_p - 0.008) + \alpha_{3,TD}\ (d_p < 8mm)$ $\alpha_{3,TD}\ (d_p > 8mm)$
α_4	$\pi\sqrt{2}/6 \approx 0.74$	$\frac{\pi/6}{5}(d_p - 0.006) + \alpha_{4,TD}\ (d_p < 6mm)$ $\alpha_{4,TD}\ (d_p > 6mm)$

3. EFFECTIVE DIAMETER

To consider the influence of particle morphology on the pressure gradients of single-phase flow, numerous prior researchers have suggested modifying the Ergun constants (C_1 and C_2) and effective diameters. The Sauter diameter of a particle is defined as the diameter of a sphere that has the same volume/surface area ratio as the particle of interest. It is expressed as follows:

$$d_{sd} = \frac{6V_p}{A_p}, \tag{17}$$

where V_p is the volume of the particle and A_p is the surface area of the particle. The equivalent diameter, which is the product of the Sauter diameter and particle shape factor, is defined as follows:

$$d_{eq} = \varphi d_{sd}. \tag{18}$$

The shape factor is the ratio of the surface area of a sphere with the same volume as the given particle to the actual surface area of the particle, and is defined as follows [9].

$$\varphi = \frac{\pi^{\frac{1}{3}}(6V_p)^{\frac{2}{3}}}{A_p}. \tag{19}$$

For the influence of particle size distribution on the pressure gradients, Li and Ma [10] and Chikhi et al. [11] organized previous studies well. They also organized the particle mean diameters for particle size distribution (mass, area, length, and number mean diameter), which are expressed as follows:

$$d_m = \sum d_j m_j = \sum \left(d_j \frac{d_j^{\,3} f_j}{\sum d_j^{\,3} f_j} \right) = \frac{\sum d_j^{\,4} f_j}{\sum d_j^{\,3} f_j}, \tag{20}$$

$$d_a = \sum d_j a_j = \sum \left(d_j \frac{d_j^{\,2} f_j}{\sum d_j^{\,2} f_j} \right) = \frac{\sum d_j^{\,3} f_j}{\sum d_j^{\,2} f_j}, \tag{21}$$

$$d_l = \sum d_j l_j = \sum \left(d_j \frac{d_j f_j}{\sum d_j f_j} \right) = \frac{\sum d_j^{\,2} f_j}{\sum d_j f_j}, \tag{22}$$

$$d_n = \sum d_j n_j = \sum \left(d_j \frac{f_j}{\sum f_j} \right) = \frac{\sum d_j f_j}{\sum f_j}. \tag{23}$$

where f_j is the number fraction of particles with a diameter of d_j in the bed, and m_j, a_j, l_j, and n_j are the weight functions by mass, area, chord length, and number of particles, respectively.

4. DESCRIPTION OF DRYOUT HEAT FLUX CALCULATION

The dryout heat flux (DHF), which is the maximum heat flux that can be removed from a unit cross-section of the debris bed, means a coolability limitation for the bed. Thus, DHF is one of the most important indicators for evaluating coolability of the debris bed on a reactor containment floor. It can be calculated by

solving the mass, momentum, and energy conservation equations. The one-dimensional, time-independent energy conservation equation is expressed as follows:

$$\frac{d}{dz}(\rho_g h_{lg} V_{sg}) = Q \cdot \tag{24}$$

where ρ_g is the gas density, h_{lg} is the evaporation latent heat, V_{sg} is the superficial gas velocity, and Q is the volumetric power density. Thus, the superficial gas velocity is calculated as follows:

$$V_{sg} = \frac{Qz}{\rho_g h_{lg}}. \tag{25}$$

The one-dimensional, time-independent mass conservation equation is expressed as follows:

$$\frac{d}{dz}(\rho_g V_{sg} + \rho_l V_{sl}) = 0 \cdot \tag{26}$$

where ρ_l is the liquid density and V_{sl} is the superficial liquid velocity. Therefore, the superficial liquid velocity is calculated as follows:

$$V_{sl} = -\frac{\rho_g}{\rho_l} V_{sg} = -\frac{Qz}{\rho_l h_{lg}}. \tag{27}$$

and if additional water inflow $V_{sl,0}$ exists from the bottom of bed, it can be expressed as follows:

$$V_{sl} = -\frac{\rho_g}{\rho_l} V_{sg} + V_{sl,0}. \tag{28}$$

The one-dimensional, time-independent momentum conservation equations for liquid and gas are expressed in Eqs. (11) and (12), and the momentum balance equation can be derived by subtracting Eq. (12) from Eq. (11) and multiplying the results by $\alpha(1-\alpha)$. It can be expressed as follows:

$$\alpha(1-\alpha) + \alpha F_{pl}^{*} - (1-\alpha) F_{pg}^{*} - F_i^{*} = 0. \tag{29}$$

For the one-dimensional steady-state boiling condition, the product of the volumetric power density Q and bed height z has a dimension of heat flux q'', which means the removable heat for a unit cross-section of the debris bed and the maximum void fraction is reached at the top of bed. Thus, the heat flux for a void fraction with a range of 0 to 1 can be calculated by solving the balance equation, Eq. (29) with the bed characteristics (porosity, particle size, and bed height) and fluid properties (density, viscosity, surface tension, and velocity), among others. The DHF is the maximum heat flux obtained by solving Eq. (29) with the void fraction at the top α, as a parameter, and the void fraction corresponding to the maximum heat flux is the actual void fraction accompanied by the DHF condition.

5. RESULTS AND DISCUSSION

5.1. Boiling Condition

For the one-dimensional steady-state boiling condition, heat transfer and phase changes exist within a bed. Therefore, a one-dimensional upward steam flow with a constant rate of flow rate increase towards the top is expected in a debris bed of uniform height with a uniform volumetric heat generation rate, in contrast to the isothermal water/air experiments. In the case of uniform power distribution, the superficial gas velocity for a given bed height z, is calculated based on the energy balance, assuming that the total heat input is used to evaporate liquid. This is expressed as $V_{sg}(z) = Qz/(\rho_g h_{lg})$, where Q is the volumetric power density and h_{lg} is the evaporation latent heat. Furthermore, the superficial liquid velocity is expressed as $V_{sl} = -\rho_g V_{sg}/\rho_l + V_{sl,0}$ by the mass conservation equation, where $V_{sl,0}$ is the superficial liquid velocity by additional inflow.
Therefore, in order to evaluate the applicability of the proposed model for pressure drop of the two-phase flow in porous media to the boiling condition, the results of DEBRIS experiments conducted at IKE in Germany [12] are compared with the analytical and proposed models. The DEBRIS experiments [12] are used to investigate the boiling, dryout, and quenching phenomena, respectively, in inductively heated particulate debris beds. Among these experiments, only the results of the boiling experiments are used for comparison with the models. For the boiling experiments, beds with a diameter of 125 mm and height of 640 mm are used. In the experiment, the pressure gradients are measured along the bed height for different heat inputs, flow modes, and system pressures. The comparable bed characteristics in the DEBRIS experiment are listed in Table III.

Table III. Characteristics of beds in DEBRIS experiment at IKE [12].

Source	Particle diameter, d_p (mm)	Porosity, ε (-)	Additional water injection, $V_{sl,0}$ (mm/s)	Pressure (bar)
Schäfer et al. [12]	3	0.4	0	1
			0.2	
			0.8	
	6	0.4	0	1
			0.2	
			0.5	

The two experimental beds consist of pre-oxidized stainless steel particles with diameters of 3 mm or 6 mm, respectively and the bed porosity is 0.4. Boiling experiments in the steady-state condition are conducted with co-current (additional water inflow from the bottom) as well as counter-current (no additional water inflow) modes at atmospheric pressure. Figs. 1–3 illustrate the dimensionless pressure gradients in each spherical particle bed in the steady-state boiling condition with/without additional water inflow, and the values predicted by the analytical and proposed models.
All symbols indicate the experimental data in spherical particle beds according to the superficial gas velocity, and it is confirmed that the influence of the interfacial drag between liquid and gas becomes larger as the particle size increases, which is the same as cases for isothermal conditions. The reduced dimensionless pressure gradient for low gas velocity is a result of the hydrostatic head reduction due to void fraction increments, according to the increasing superficial gas velocity. When the dimensionless pressure gradient reaches the nearly minimum value, it remains almost constant, as the particle-gas drag increment compensates for the hydrostatic head reduction. Thereafter, it increases steadily as the superficial gas velocity increases, because the rate of increase in the particle-gas drag is faster than the hydrostatic head reduction.

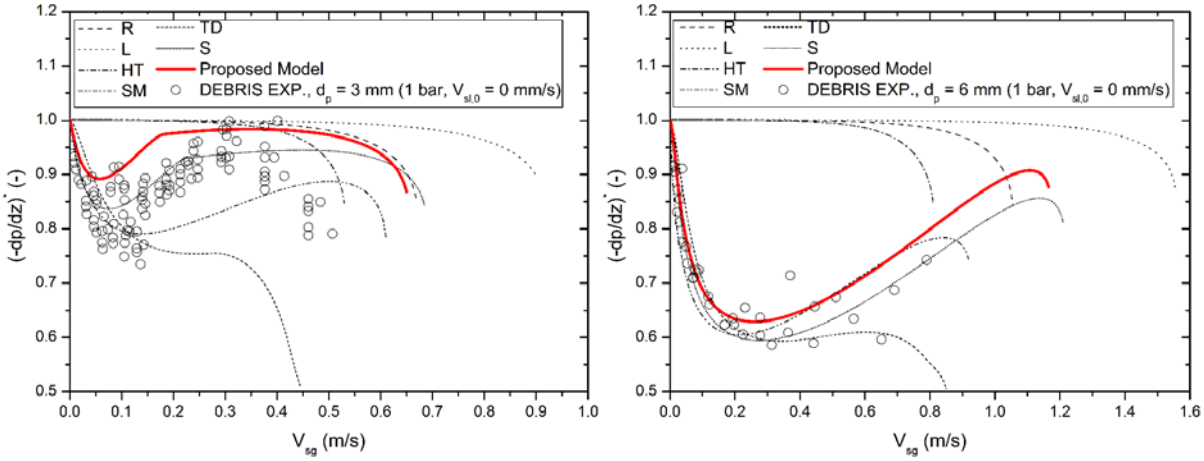

(a) 3 mm in diameter **(b) 6 mm in diameter**

Figure 1. Dimensionless pressure gradients in spherical particle beds in steady-state boiling condition with no additional water inflow, and the values predicted by existing and proposed models: (a) 3 mm, (b) 6 mm [12].

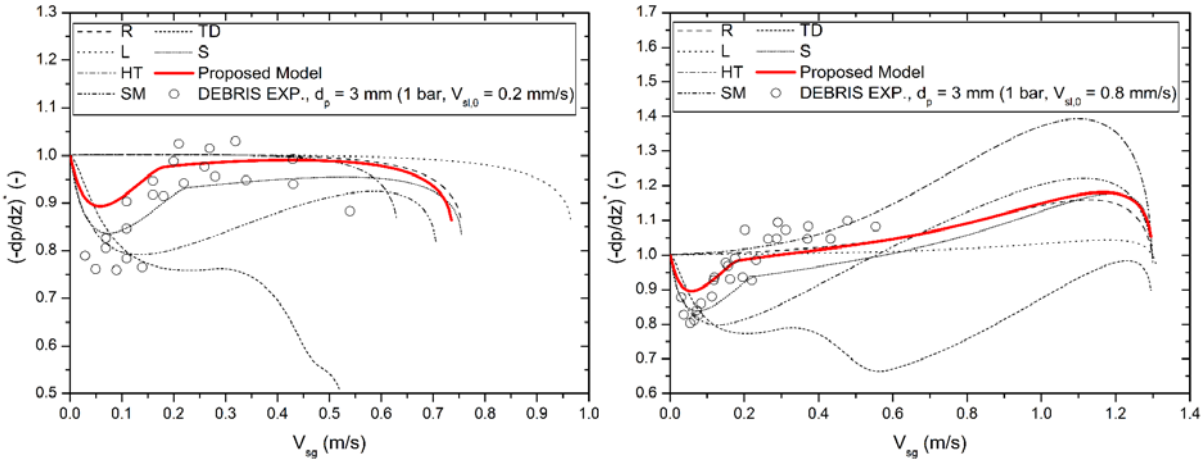

(a) $V_{sl,0}$ = 0.2 mm/s **(b) $V_{sl,0}$ = 0.8 mm/s**

Figure 2. Dimensionless pressure gradients in spherical particle bed (3 mm) in steady-state boiling condition with additional water inflow, and the values predicted by existing and proposed models: (a) $V_{sl,0}$ = 0.2 mm/s, (b) $V_{sl,0}$ = 0.8 mm/s [12].

In particular, Fig. 1(a) shows that the pressure gradients decrease above the superficial gas velocity of 0.3 m/s. In this range, annular flow is developed due to the significantly high void, and liquid flow is extremely limited, resulting in increased particle friction and decreased pressure gradients.

In Figs. 1–3, the curves represent the values predicted by the analytical (Reed, R [13]; Lipinski, L [14]; Hu and Theofanous, HT [15]; Schulenberg and Müller, SM [16]; Tung and Dhir, TD [8]; and Schmidt, S [5]) and proposed models. It can be seen that the models that exclude the interfacial drag between liquid and gas (Reed [13], Lipinski [14], and Hu and Theofanous [15]) do not predict the pressure gradients, and it remains at the hydrostatic pressure gradient level, $(-dp/dz)^* = 1$ in the lower superficial gas velocity region. However, the models that consider the interfacial drag (Schulenberg and Müller [16], Tung and Dhir [8], and Schmidt [5]) and the proposed model predict the pressure gradients in the lower superficial gas velocity region.

Overall, for the spherical particle bed with 3 mm diameters (Figs. 1(a) and 2), Schmidt and the proposed model predict the pressure gradients effectively. For the spherical particle bed with 6 mm diameters (Figs.

1(b) and 3), Schulenberg and Müller [16], Schmidt [5], and the proposed model predict the pressure gradients effectively. As the measured pressure gradient fluctuations are quite large, it is difficult to determine which model among Schulenberg and Müller [16], Schmidt [5], and the proposed model is most suitable for predicting the pressure gradients through each spherical particle bed in the boiling condition with/without additional water inflow; however, the applicability of the proposed model is confirmed.

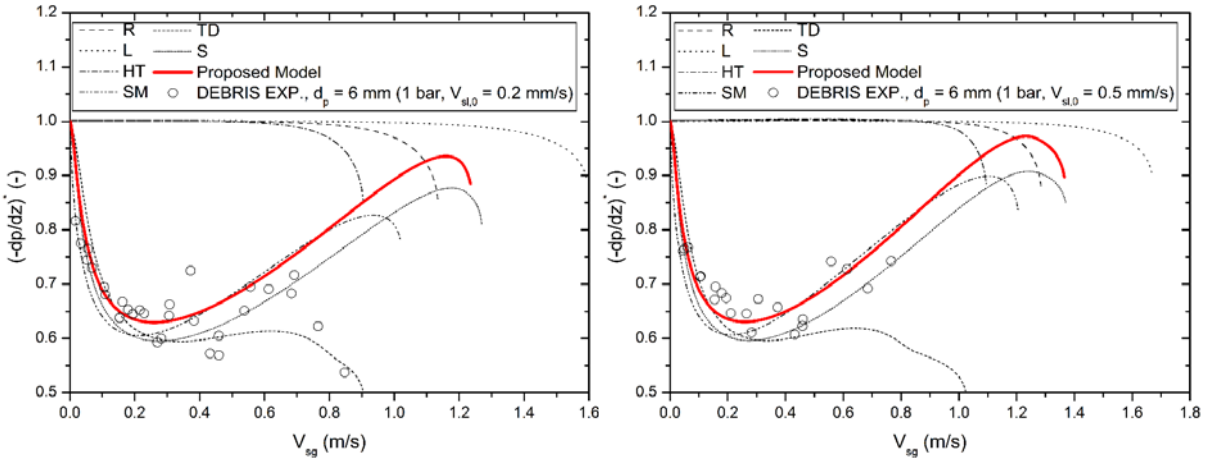

(a) $V_{sl,0}$ = 0.2 mm/s **(b) $V_{sl,0}$ = 0.5 mm/s**

Figure 3. Dimensionless pressure gradients in spherical particle bed (6 mm) in steady-state boiling condition with additional water inflow, and the values predicted by existing and proposed models: (a) $V_{sl,0}$ = 0.2 mm/s, (b) $V_{sl,0}$ = 0.5 mm/s [12].

5.2. Dryout Heat Flux

In order to evaluate the applicability of the proposed model to the pressure drop of two-phase flow through porous media in DHF prediction, the results of the DEBRIS experiments conducted at IKE in Germany [12, 17, 18] and those by Bang and Kim [19] are compared with the analytical and proposed models. The characteristics of comparable beds for the DHF experiments are listed in Table IV. For the case of comparable beds by Schäfer et al. [12], the measured DHF was compared to the values predicted by the models to evaluate the particle size (3 and 6 mm) effect on DHF, and the experimental cases by Leininger et al. [17] and Rashid et al. [18] were used for evaluating the adequacy of the effective diameter for non-spherical particles (cylindrical particles with a diameter of 3 mm and length of 5.75 mm) or poly-dispersed spherical particles (2, 3 and 6 mm with mass ratio of 2:3:5; d_m: 4.30 mm, d_a: 3.53 mm, d_l: 2.91 mm, and d_n: 2.53 mm), with system pressure effect (1, 3, 5 bar) on DHF. Furthermore, the experimental cases by Bang and Kim [19] were compared in order to investigate the influences of the particle size and additional water injection rate on DHF.

Table IV. Characteristics of comparable beds for DHF experiments.

Source	Particle size, d_p (mm)	Porosity, ε (-)	Bed height, z (cm)	Additional water injection, $V_{sl,0}$ (m/s)	Pressure (bar)
Schäfer et al. [12]	$d_p = 3$	0.4	64	0	1
	$d_p = 6$	0.4	64	0	1
Leininger et al. [17]	$d_{eq} = 2.99$	0.38	64	0	1, 3, 5
Rashid et al. [18]	$d_a = 3.53$	0.37	64	0	1, 3, 5
Bang and Kim [19]	$d_p = 3.2$	0.37	30	$0 - 1.05 \times 10^{-3}$	1
	$d_p = 4.8$	0.38	30	$0 - 1.57 \times 10^{-3}$	1

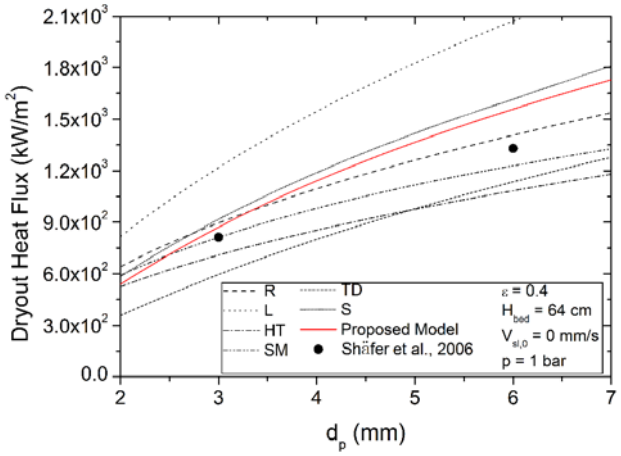

Figure 4. Dryout heat flux in spherical particle beds (d_p = 3, 6 mm) without additional water inflow at 1 bar by Schäfer et al. [12], and the values predicted by existing and proposed models.

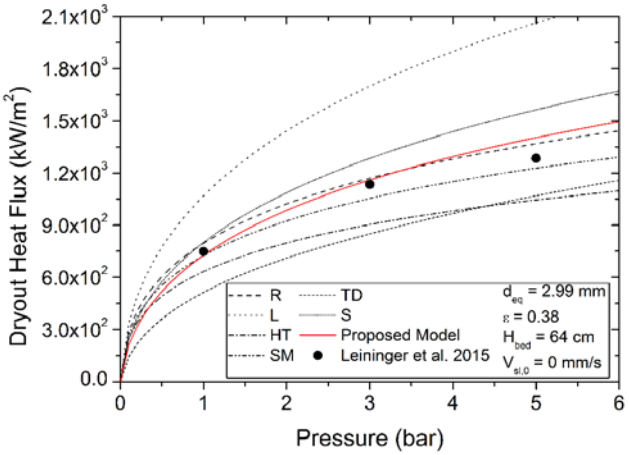

Figure 5. Dryout heat flux in cylindrical particle bed (d_{eq} = 2.99 mm) without additional water inflow by Leininger et al. [17], and the values predicted by existing and proposed models.

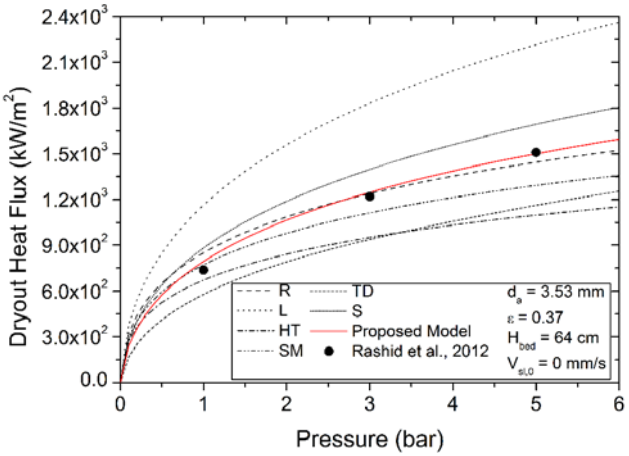

Figure 6. Dryout heat flux in poly-dispersed particle bed (d_a = 3.53 mm) without additional water inflow at 1–5 bar by Rashid et al. [18], and the values predicted by existing and proposed models.

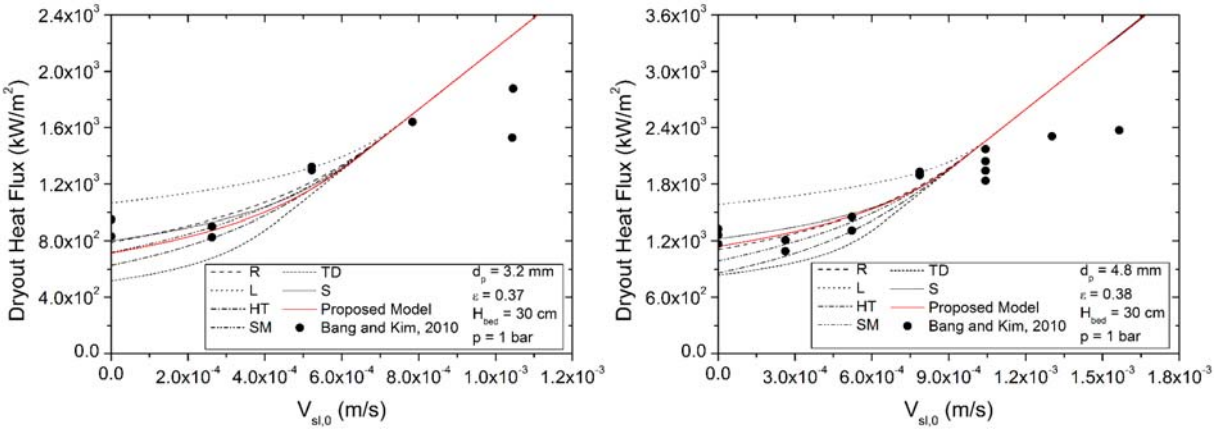

(a) 3.2 mm in diameter **(b) 4.8 mm in diameter**

Figure 7. Dryout heat flux in spherical particle beds (d_p = 3.2 and 4.8 mm) with additional water inflow at 1 bar by Bang and Kim [19], and the values predicted by existing and proposed models.

Figs. 4–7 illustrate the DHF in each comparable bed under various conditions, with the values predicted by the analytical and proposed models. All symbols show the DHF in comparable beds, and the curves represent the values predicted by the analytical (Reed, R [13]; Lipinski, L [14]; Hu and Theofanous, HT [15]; Schulenberg and Müller, SM [16]; Tung and Dhir, TD [8]; and Schmidt, S [5]) and proposed models. It is confirmed that the DHF increases with an increment in particle diameter, system pressure, and additional water inflow rate. Overall, for the comparable experimental cases for DHF, Reed [13], Schulenberg and Müller [16], Schmidt [5], and the proposed models predict DHF effectively. However, since the Reed model does not consider the interfacial drag, there is a limit to evaluating the long-term cooling performance. This is because in the long-term cooling view, with a bubbly or slug flow regime, the effect of the interfacial drag cannot be ignored and will appear. Furthermore, in the case of the Schulenberg and Müller model [16], the interfacial drag was considered, but only the relative gas passability reflects the influence of the flow regime on the basis of a void fraction of 0.3, and the remaining parameters have limitations, because the influence of the flow regime is not reflected. In the case of the Schmidt model [5], the Tung and Dhir model [8] was improved to predict the pressure drop in particle beds composed of relatively small particles more effectively, but the Schmidt model [5] exhibits limitations in predicting the pressure drop in particle beds with a particle size of less than 6 mm. Therefore, the applicability of the proposed model is verified with the effective mean diameter (equivalent diameter for non-spherical particles and area mean diameter for size-distributed particles). In the case of additional water inflow conditions [19] as illustrated in Fig. 7, the proposed model is applicable to predict one-dimensional DHF in beds up to approximately $V_{sl,0}$ of 1 mm/s.

6. CONCLUSIONS

To evaluate the adequacy of a new two-phase pressure drop model [3] for porous media with the effective diameter for non-spherical particles under boiling conditions and dryout heat flux prediction, the present study was performed. The proposed by our previous study verified by existing various experimental data with the diameter of 3.18–6.35 mm in the superficial air velocity range of 0–0.8 m/s under isothermal conditions. The comparison between the experimental data (pressure drop in boiling condition and dryout heat flux) and the values predicted by the proposed model was conducted using the various results of DEBRIS experiments conducted at IKE in Germany and others using spherical and cylindrical particles with/without size distribution. In conclusion, the adequacy of the proposed model for predicting the pressure drop of the two-phase flow in particle beds with the effective mean diameter (equivalent diameter for non-spherical particles and area mean diameter for size-distributed particles) was verified under boiling

conditions as well as dryout heat flux prediction with/without additional water injection up to approximately $V_{sl,0}$ of 1 mm/s.

ACKNOWLEDGMENTS

This work was supported by the Nuclear Safety Research Program through the Korea Foundation Of Nuclear Safety(KoFONS) using the financial resource granted by the Nuclear Safety and Security Commission(NSSC) of the Republic of Korea. (No. 1805001).

REFERENCES

1. Moriyama, K., et al., *Coarse break-up of a stream of oxide and steel melt in a water pool(contract research).* JAERI-Research, 2005. **2005**: p. 017.
2. Magallon, D., *Characteristics of corium debris bed generated in large-scale fuel-coolant interaction experiments.* Nuclear Engineering and Design, 2006. **236**(19-21): p. 1998-2009.
3. Park, J.H., et al., *Modeling of pressure drop in two-phase flow of mono-sized spherical particle beds.* International Journal of Heat and Mass Transfer, 2018. **127**: p. 986-995.
4. Park, J.H., et al., *Influence of Particle Morphology on Pressure Gradients of Single-Phase Air Flow in the Mono-Size Non-Spherical Particle Beds.* Annals of Nuclear Energy, 2018. **115**: p. 1-8.
5. Schmidt, W., *Influence of multidimensionality and interfacial friction on the coolability of fragmented corium.* 2004.
6. Carman, P.C., *Fluid flow through granular beds.* Transactions-Institution of Chemical Engineeres, 1937. **15**: p. 150-166.
7. Bo-Ming, Y. and L. Jian-Hua, *A geometry model for tortuosity of flow path in porous media.* Chinese Physics Letters, 2004. **21**(8): p. 1569.
8. Tung, V. and V. Dhir, *A hydrodynamic model for two-phase flow through porous media.* International journal of multiphase flow, 1988. **14**(1): p. 47-65.
9. Wadell, H., *Volume, shape, and roundness of quartz particles.* The Journal of Geology, 1935: p. 250-280.
10. Li, L. and W. Ma, *Experimental characterization of the effective particle diameter of a particulate bed packed with multi-diameter spheres.* Nuclear Engineering and Design, 2011. **241**(5): p. 1736-1745.
11. Chikhi, N., et al., *Evaluation of an effective diameter to study quenching and dry-out of complex debris bed.* Annals of Nuclear Energy, 2014. **74**: p. 24-41.
12. Schäfer, P., M. Groll, and R. Kulenovic, *Basic investigations on debris cooling.* Nuclear Engineering and Design, 2006. **236**(19-21): p. 2104-2116.
13. Reed, A.W., *The effect of channeling on the dryout of heated particulate beds immersed in a liquid pool*. 1982, Massachusetts Institute of Technology.
14. Lipinski, R.J., *Model for boiling and dryout in particle beds. [LMFBR]*. 1982. p. Medium: X; Size: Pages: 177.
15. Hu, K. and T. Theofanous, *On the measurement and mechanism of dryout in volumetrically heated coarse particle beds.* International journal of multiphase flow, 1991. **17**(4): p. 519-532.
16. Schulenberg, T. and U. Müller, *An improved model for two-phase flow through beds of coarse particles.* International journal of multiphase flow, 1987. **13**(1): p. 87-97.
17. Leininger, S., R. Kulenovic, and E. Laurien. *Experimental investigations on the coolability of stratified debris beds*. in *7th European Review Meeting on Severe Accident Research (ERMSAR-2015), Marseille, Frankreich*. 2015.
18. Rashid, M., R. Kulenovic, and E. Laurien, *Experimental results on the coolability of a debris bed with down comer configurations.* Nuclear Engineering and Design, 2012. **249**: p. 104-110.
19. Bang, K.-H. and J.-M. Kim, *Enhancement of dryout heat flux in a debris bed by forced coolant flow from below.* Nuclear Engineering and Technology, 2010. **42**(3): p. 297-304.